

## Supplementary Material

# **Trimming defective perovskite layer surface for high-performance solar cells**

Chanhyeok Kim<sup>1</sup>, Kihoon Kim<sup>1</sup>, Youngmin Kim<sup>1</sup>, Nikolai Tsvetkov<sup>1</sup>, Nam Joong Jeon<sup>2</sup>, Bong Joo Kang<sup>2,\*</sup>, Hanul Min<sup>1,3,4,\*</sup>

*<sup>1</sup>KU-KIST Graduate School of Converging Science and Technology, Korea University, Seoul, South Korea*

*<sup>2</sup>Division of Advanced Materials, Korea Research Institute of Chemical Technology, Daejeon, South Korea*

*<sup>3</sup>Department of Integrative Energy Engineering, Korea University, Seoul, South Korea*

*<sup>4</sup>Clean Energy Research Center, Korea Institute of Science and Technology, Seoul, South Korea*

*\*To whom correspondence should be addressed. E-mail: [bjkang@kricr.re.kr](mailto:bjkang@kricr.re.kr); [hmin92@korea.ac.kr](mailto:hmin92@korea.ac.kr)*

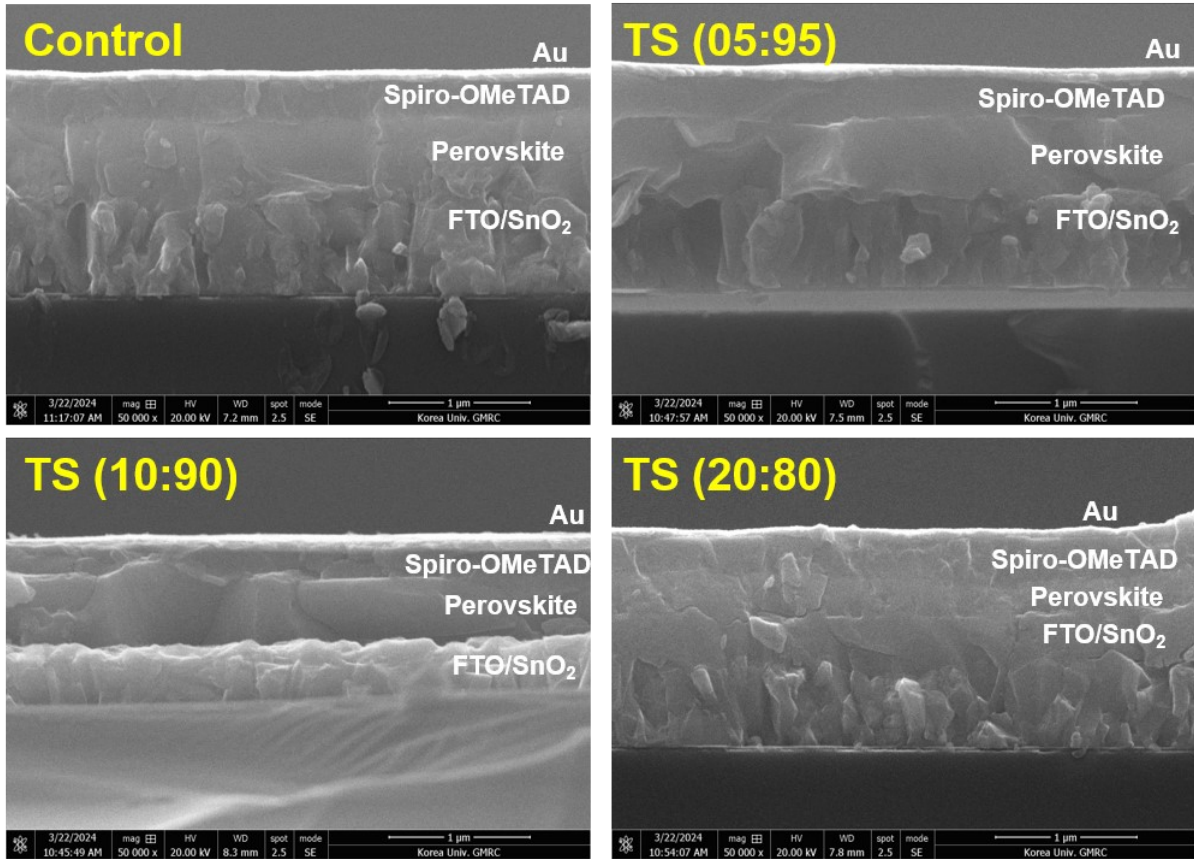


**Fig. S1.** Cross-sectional SEM images of the control, TS (05:95), TS (10:90), and TS (20:80) devices.

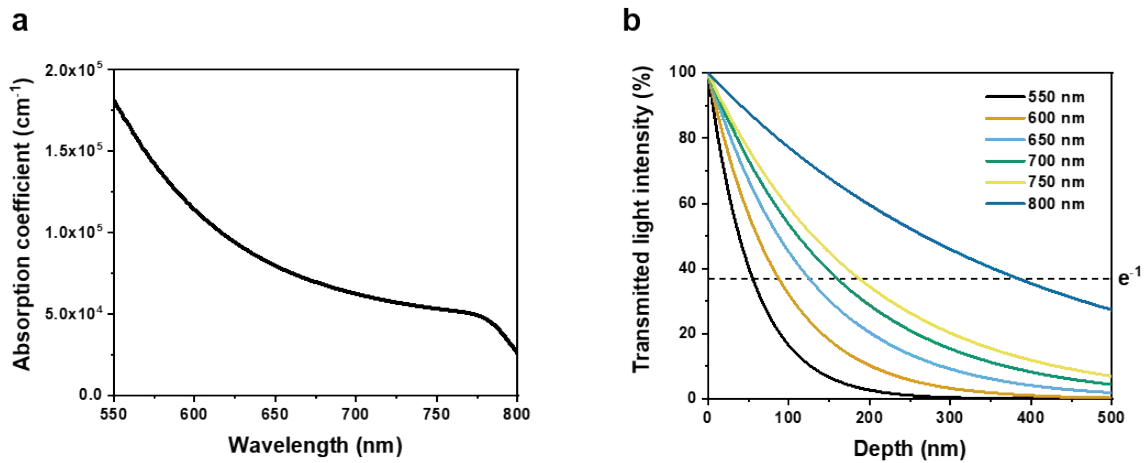


**Fig. S2.** (a) Absorption coefficient of the perovskite layer and (b) transmitted light intensity for different wavelengths.

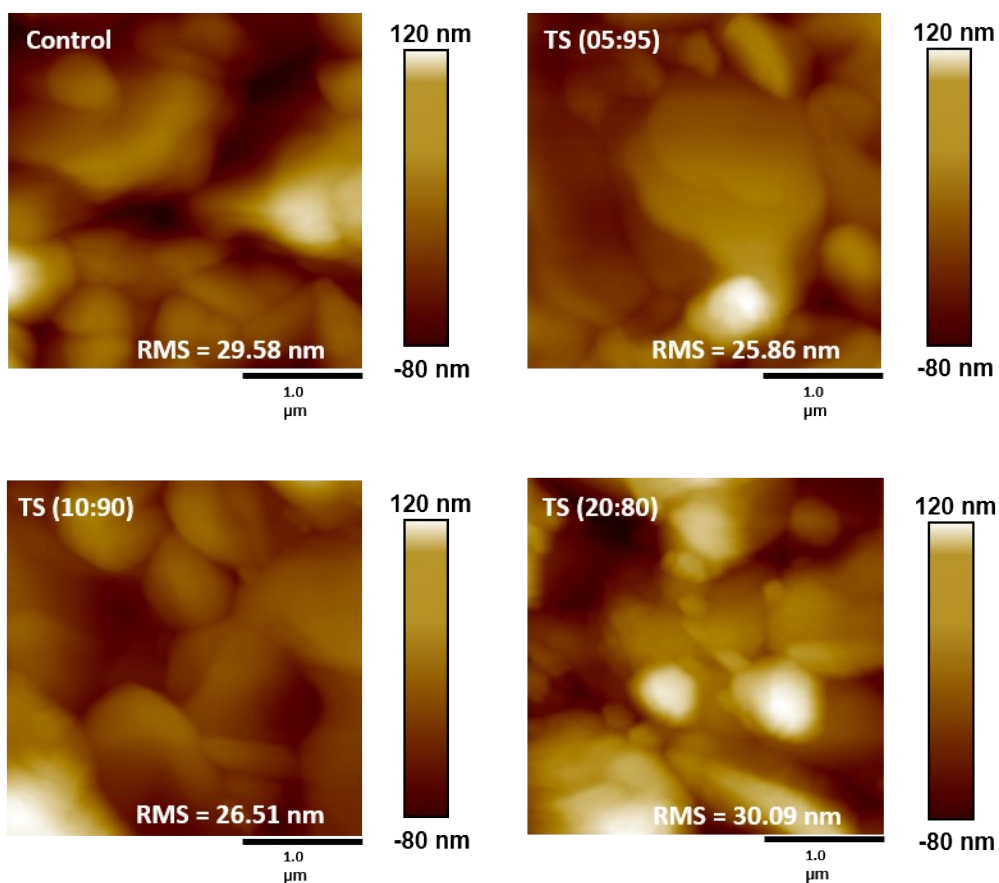


Fig. S3. Atomic force microscopy images of the control, TS (05:95), TS (10:90), and TS (20:80) perovskite thin films.

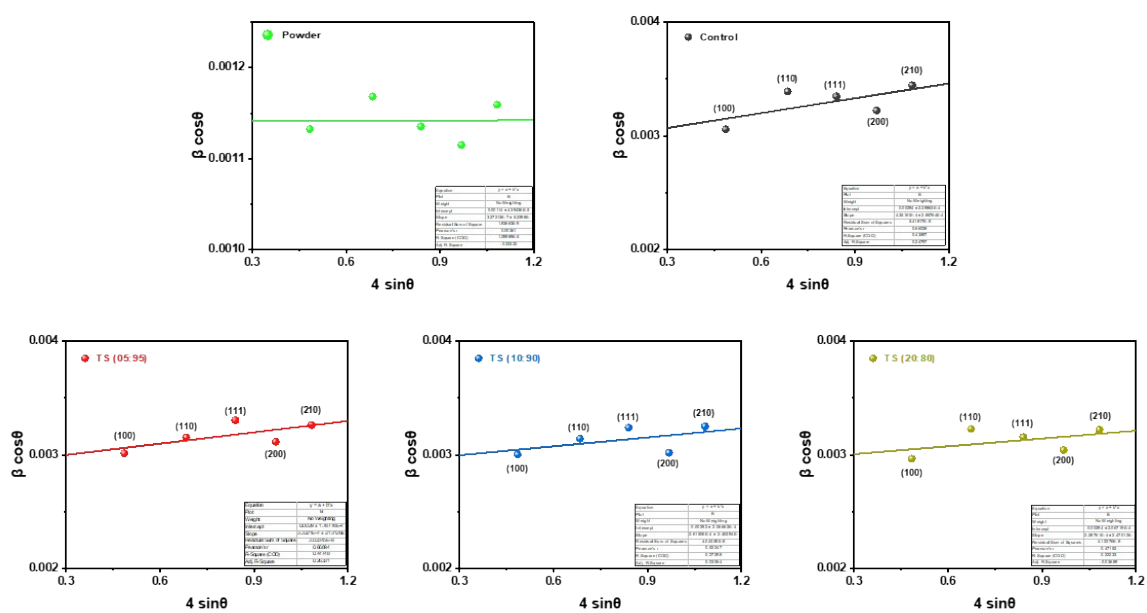
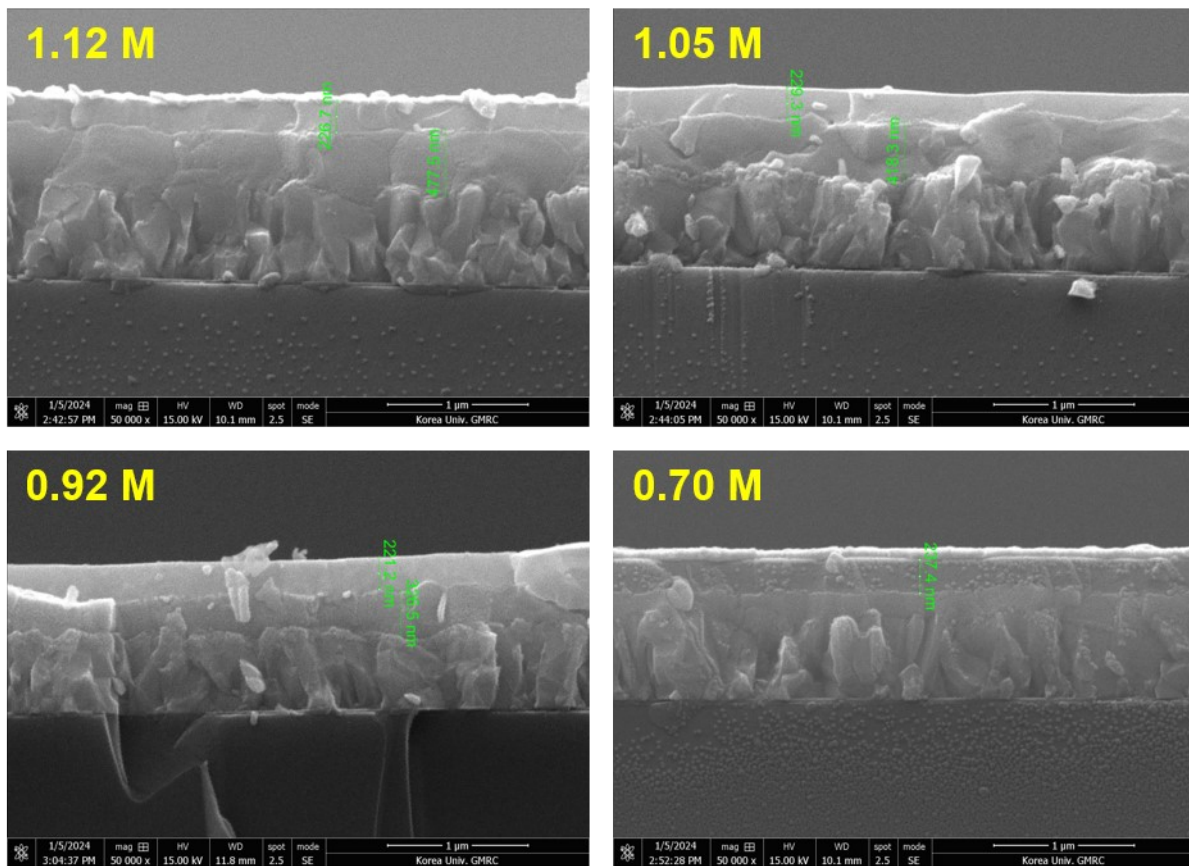


Fig. S4. Williamson-Hall plots of the control, TS (05:95), TS (10:90), and TS (20:80) perovskite thin films.



**Fig. S5.** Cross-sectional SEM images of the perovskite film for different perovskite precursor concentrations.

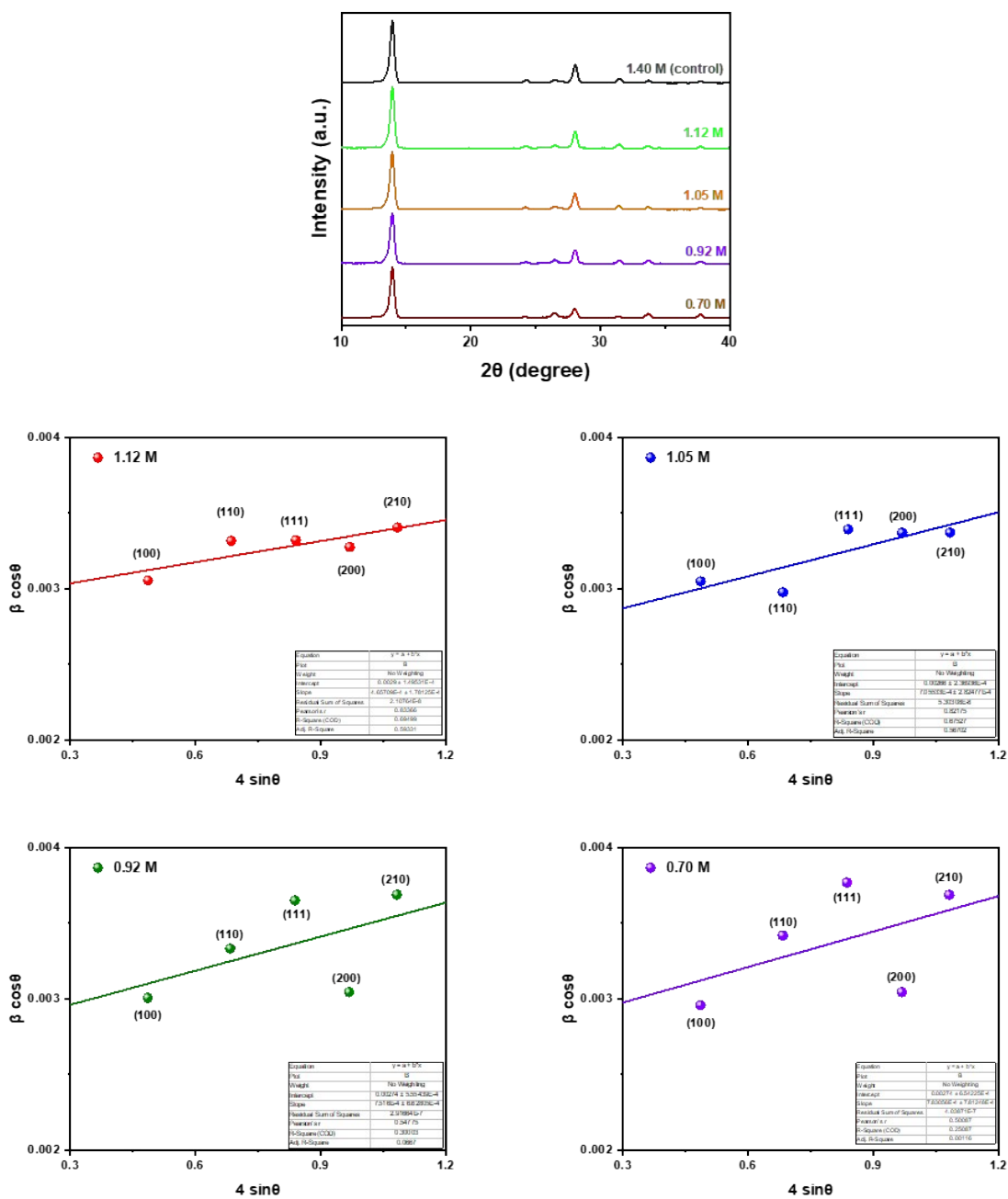
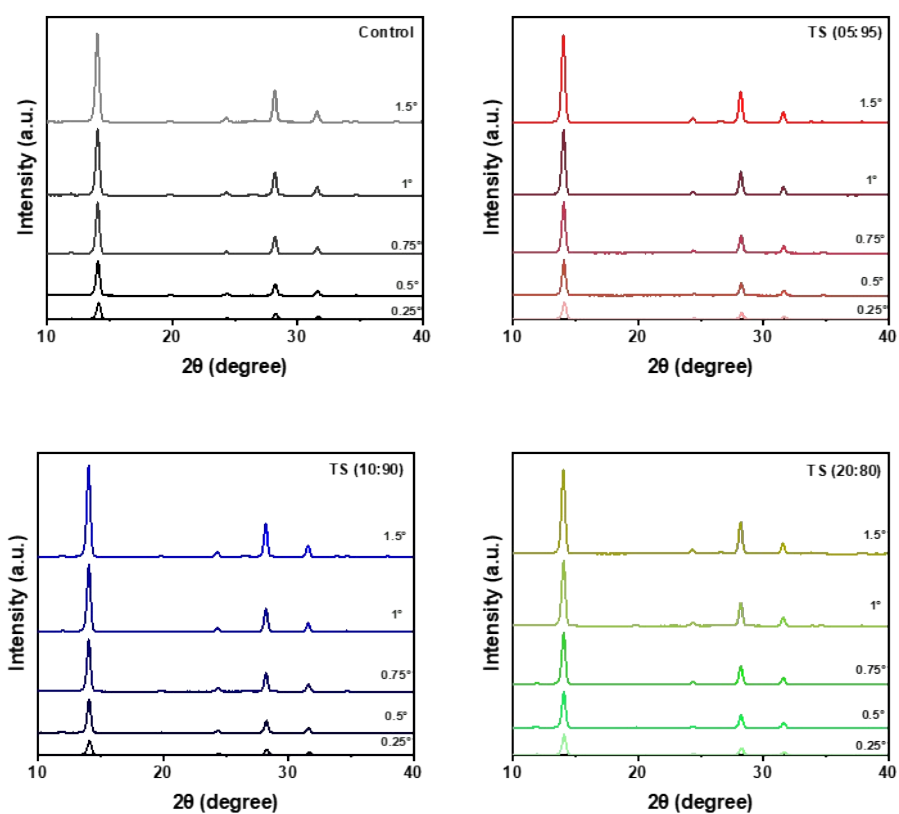
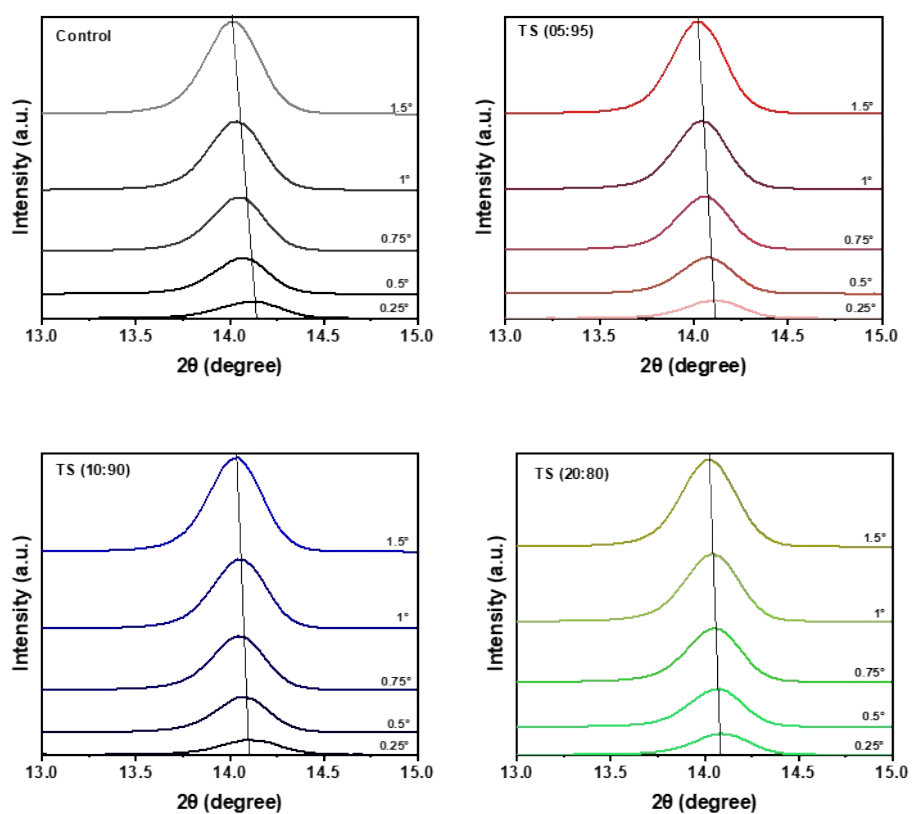


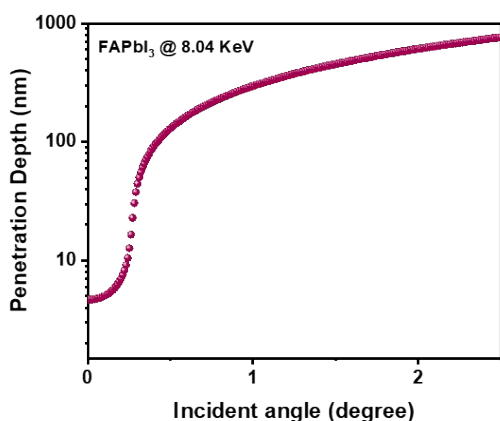
Fig. S6. XRD patterns and individual Williamson-Hall plot of the perovskite thin films prepared with 1.40 M, 1.12 M, 1.05 M, 0.92 M, and 0.70 M of FAPbI<sub>3</sub>.



**Fig. S7. GIXRD patterns of the control, TS (05:95), TS (10:90), and TS (20:80) perovskite thin films at different incidence angles.**



**Fig. S8. Magnified GIXRD peaks corresponding to the (100) plane of the control, TS (05:95), TS (10:90), and TS (20:80) perovskite films at varying incidence angles.**



Grazing incident angle (degree)	Penetration depth (nm)
0.25	12.7
0.5	123.8
0.75	217.1
1	298.2
1.5	456.47
2	612.8

\*Density of FAPbI<sub>3</sub>,  $d=4.101\text{g/cm}^3$ ,  
From *Inorg. Chem.* 2013, 52, 9019-9038

**Fig. S9. X-ray penetration depth  $\Lambda$  into the FAPbI<sub>3</sub> layer at different incidence angles,**

calculated as:

$$\Lambda = \frac{\lambda}{\sqrt{2\pi}} \times \frac{1}{\sqrt{\sqrt{(\alpha_i^2 - \alpha_c^2)^2 + 4\beta^2} - (\alpha_i^2 - \alpha_c^2)}}$$

where  $\alpha_i$  is the incidence angle,  $\alpha_c$  is the critical angle of the sample,  $\lambda$  is the X-ray wavelength, and  $\beta$  is the imaginary part of the refraction index, defined as  $n = 1 - \delta + i\beta$ . The  $\delta$  and  $\beta$  parameters for FAPbI<sub>3</sub> at 8.04 keV ( $\lambda = 1.54 \text{ \AA}$ ) were  $1.08329 \times 10^{-5}$  and  $1.22906 \times 10^{-6}$ , respectively, as determined using the online toolbox available at [https://henke.lbl.gov/optical\\_constants/getdb2.html](https://henke.lbl.gov/optical_constants/getdb2.html).



**Table S1.** Microstrains calculated from the GIXRD patterns of the control, TS (05:95), TS (10:90), and TS (20:80) thin films at different incidence angles.

<b>Incidence angle</b>	<b>0.25° (<math>\epsilon \times 10^4</math>)</b>	<b>0.5° (<math>\epsilon \times 10^4</math>)</b>	<b>0.75° (<math>\epsilon \times 10^4</math>)</b>	<b>1° (<math>\epsilon \times 10^4</math>)</b>	<b>1.5° (<math>\epsilon \times 10^4</math>)</b>
<b>Control</b>	4.3223	3.8565	1.9579	0.3856	0.2551
<b>TS (05:95)</b>	3.9907	2.9453	1.7198	0.3545	0.2537
<b>TS (10:90)</b>	3.2813	2.8302	1.4861	0.3249	0.2586
<b>TS (20:80)</b>	2.7364	2.1199	1.2695	0.3105	0.2547

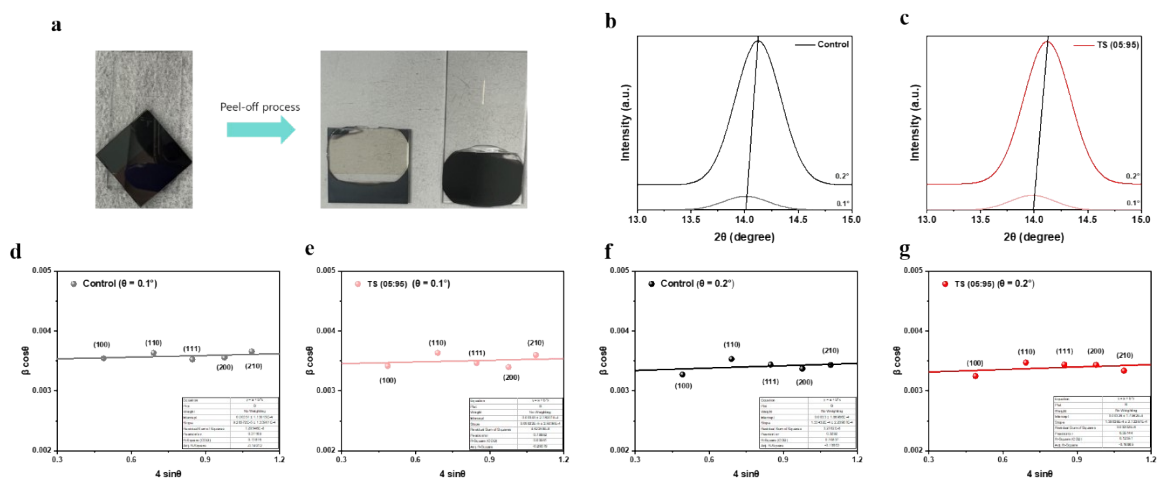


**Fig. S10.** (a) Perovskite film peeled-off from the substrate. (b-c) Magnified GIXRD diffraction peaks corresponding to the (100) plane of the buried interface. (d-g) WH plots of the buried interface of the control and TS (05:95).

**Table S2.** Microstrains calculated from the GIXRD patterns of the buried interface of the control and TS (05:95) thin films at different incidence angles.

Incidence angle	0.1° ( $\epsilon \times 10^4$ )	0.2° ( $\epsilon \times 10^4$ )
Control	0.9285	1.3343
TS (05:95)	0.9099	1.3802

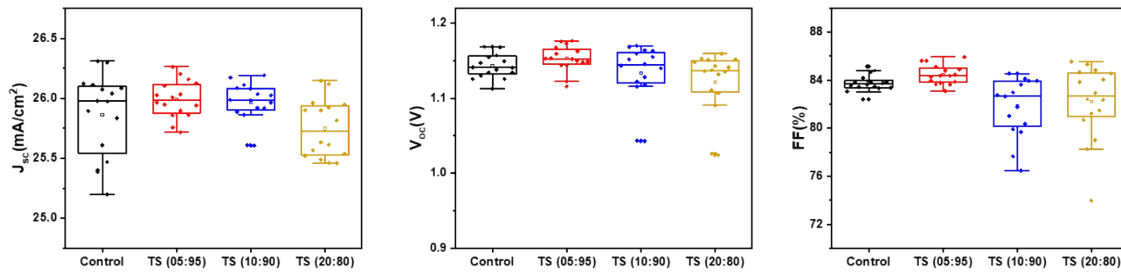
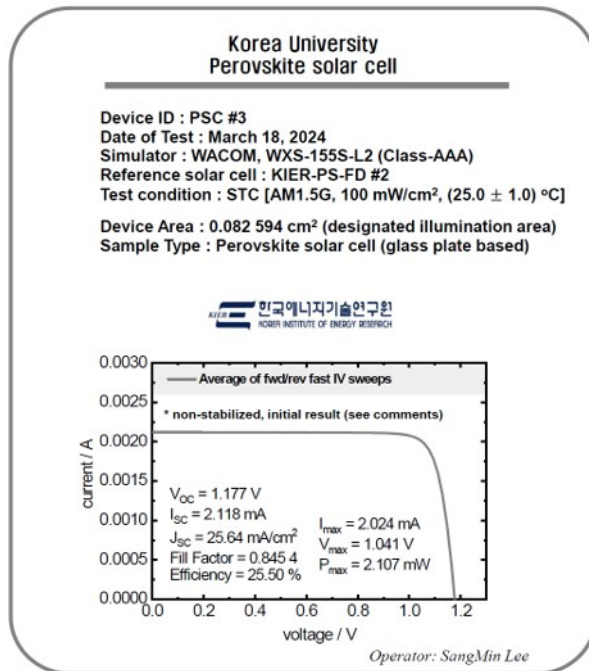


Fig. S11. Statistics of key performance parameters of the control, TS (05:95), TS (10:90), and TS (20:80) devices.

[Appendix 1]



Photovoltaics Research Department, Korea Institute of Energy Research  
 152, Gajeong-ro, Yuseong-gu, Daejeon, 34129, Korea  
 Tel : +82-42-860-3182, e-mail : notask@kier.re.kr

Fig. S12. Independent PCE certification issued by the Korea Institute of Energy Research.

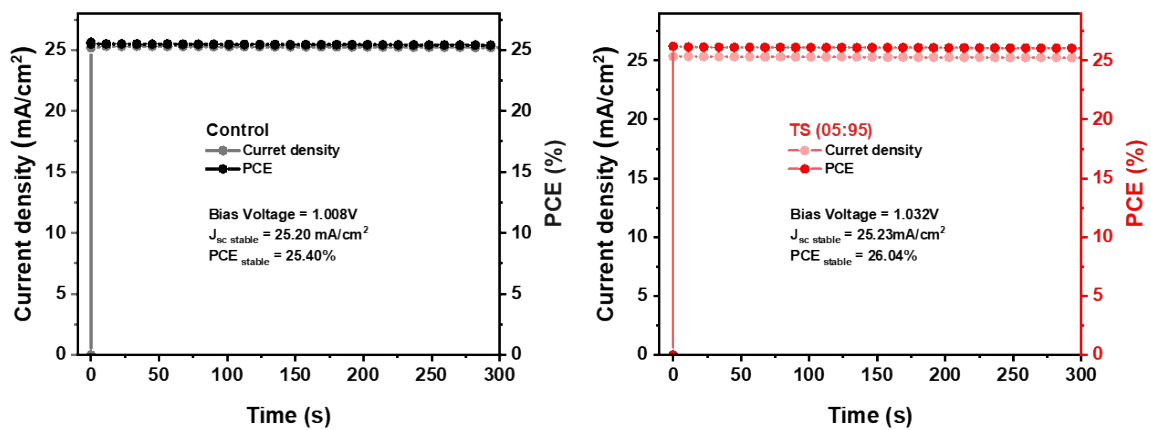


**Fig. S13.** Stabilized power output and current density at the maximum power point for the control and TS (05:95) devices.

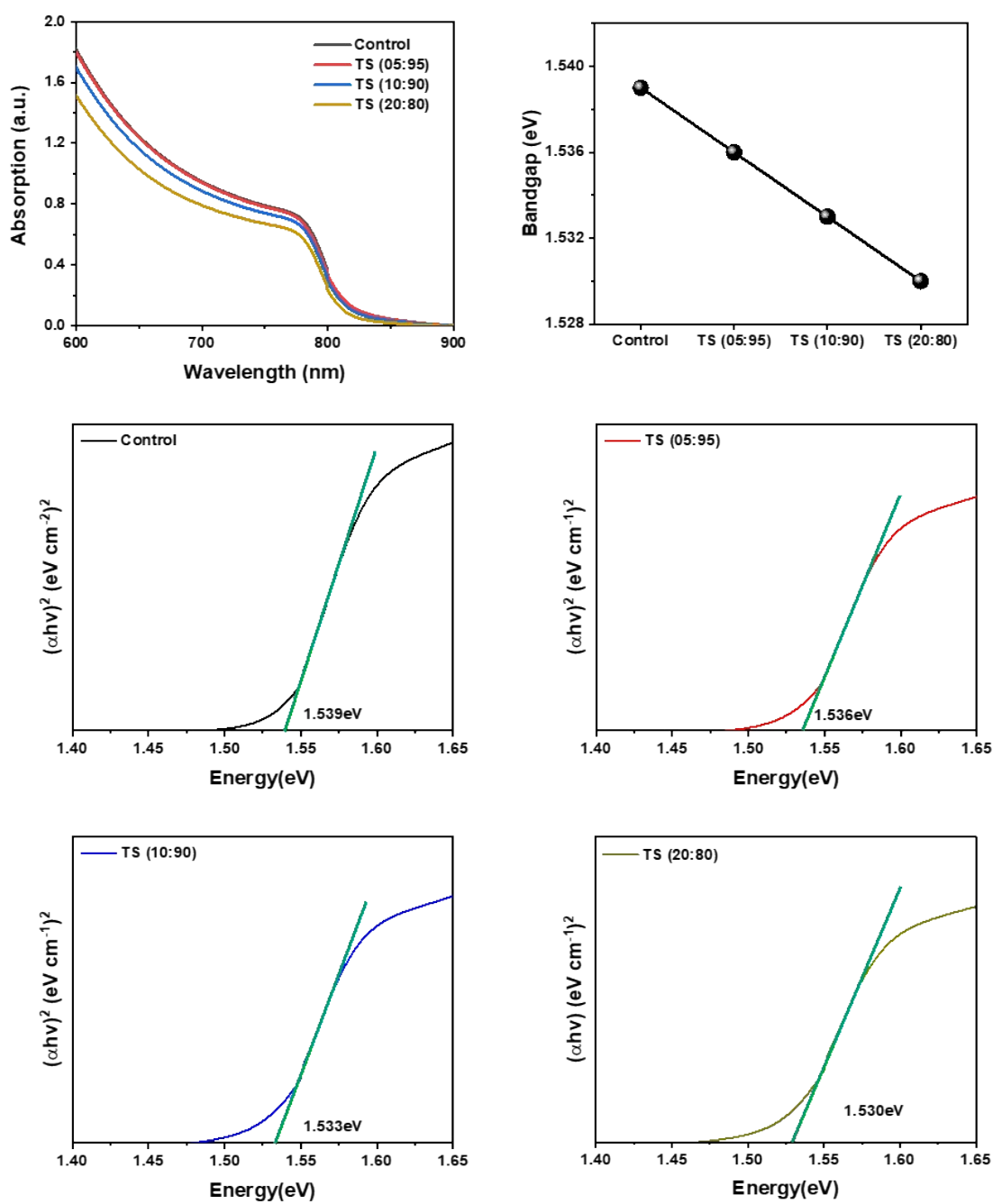


**Fig. S14. UV-vis absorption spectra and bandgaps of the control, TS (05:95), TS (10:90), and TS (20:80) perovskite thin films.**

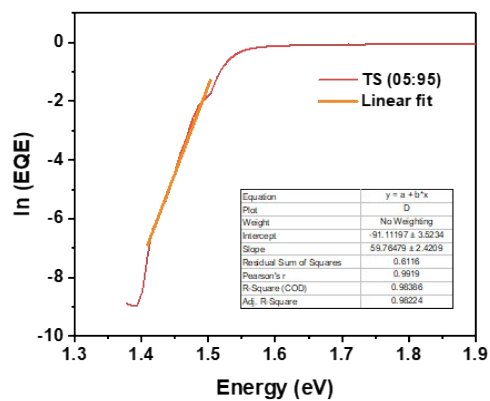
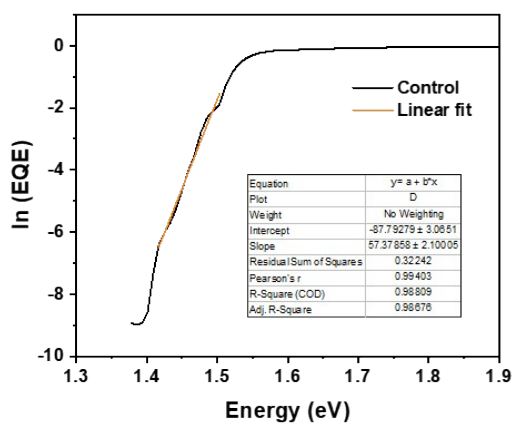


Fig. S15. Semilog EQE vs photon energy for the control and TS (05:95) devices.